JACS
JOURNAL OF THE AMERICAN CHEMICAL SOCIETY

Article

pubs.acs.org/JACS

Helical Self-Assembly-Induced Singlet–Triplet Emissive Switching in a Mechanically Sensitive System

Hongwei Wu,[†] Yunyun Zhou,[‡] Liyuan Yin,[‡] Cheng Hang,[‡] Xin Li,[§] Hans Ågren,[§] Tao Yi,[∥] Qing Zhang,*[,†] and Liangliang Zhu*[,‡]

[†]Shanghai Key Laboratory of Electrical Insulation and Thermal Aging, School of Chemistry and Chemical Engineering, Shanghai Jiaotong University, Shanghai 200240, China

[‡]State Key Laboratory of Molecular Engineering of Polymers, Department of Macromolecular Science, Fudan University, Shanghai 200433, China

[§]Division of Theoretical Chemistry and Biology School of Biotechnology, KTH Royal Institute of Technology, SE-10691 Stockholm, Sweden

[∥]Department of Chemistry and Collaborative Innovation Center of Chemistry for Energy Materials, Fudan University, Shanghai 200433, China

Supporting Information

ABSTRACT: In nanoscience, chirality has shown a significant ability to tune materials' electronic properties, whereas imposing macrochirality into the regulation of singlet–triplet features of organic optoelectronics remains a challenging research topic. Since the tuning for singlet and triplet excited-state properties in a single π-functional molecule connects to its multicolor luminescent application and potential improvement of internal quantum efficiency, we here report that supramolecular chirality can be employed to toggle the singlet and triplet emissions in a well-designed asterisk-shaped molecule. Employing a hexathiobenzene-based single luminophore as a prototype and functionalizing it with chiral α-lipoiate side groups, we find that helical nanoarchitectures can accordingly form in mixed DMF/H_2O solution. On this basis, switching between fluorescence and phosphorescence of the material can be realized upon helical self-assembly and dissociation. Such a behavior can be attributed to a helical-conformation-dependent manipulation of the intersystem crossing. Furthermore, reversible mechanoluminescence of the corresponding solid sample was also observed to rely on an analogous molecular self-assembly alternation. These results can probably provide new visions for the development of next-generation supramolecular chiral functional materials.

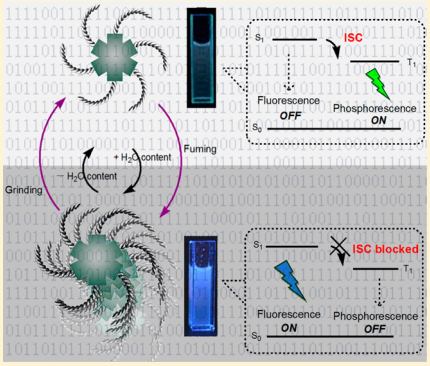

INTRODUCTION

Chirality continues to attract attention in diverse areas of modern material science, as studies of this concept can help us better understand the nature of new-generation advanced functional nanomaterials.[1] In particular, supramolecular chirality originating from helical self-assemblies normally produces distinct properties, different from those of the single constituent molecules.[2] The past decade has witnessed extensive progress in the nanoengineering of chiral self-assemblies, the application of which has been largely focused on the morphology, dynamics, biological and electronic functions of the regulating materials.[3] However, facile tuning of the light-emitting properties in organic luminophores by supramolecular chirality has been relatively little attended. Although the singlet or triplet excited-state properties of π-functional molecules can generally respond to a variety of molecular stacking factors,[4] to the best of our knowledge, rational design of systems whose singlet–triplet (S–T) emissions can be toggled efficiently via helical self-assembly remains a challenge.

Since fluorescence and phosphorescence in a single system can cover individual visible-light spectral regions due to their significant energy difference, the S–T emissive switching is regarded as one of important perspectives for the development of intelligent luminescent materials. Fluorescence–phosphorescence dual emission phenomena have been observed in a few materials related to structure-dependent molecular stacking,[5] Nevertheless, a deep control of S–T emissive switching at the unimolecular level requires more precise self-assembly pathways. On this basis, we propose a unimolecular strategy of harnessing helical self-assembly for realization of the controllable S–T emission via toggling between fluorescence and phosphorescence. The strategy is inspired by that supramolecular chirality can significantly extend π-electron delocalization so as to enlarge or metamorphose pertinent functions.[4,5] Our idea is to employ a tunable helical self-assembly to regulate molecular energy levels and intersystem crossing (ISC)[6] in

Received: October 7, 2016
Published: December 27, 2016

DOI: 10.1021/jacs.6b10550
J. Am. Chem. Soc. 2017, 139, 785–791

order to switch between singlet and triplet emission at the single luminophore level.

Persulfurated aromatic molecules have attracted attentions due to a variety of their exalted photophysical properties.[7] Recently, this kind of structures has been found to be an effective metal-free room-temperature phosphorescence emitter with a tunable ISC process under constrained environments.[8] These compounds can be easily synthesized from cheap and commercially available starting materials with particular modifications by different functional groups for postprocessing.[9] In this work, a novel asterisk-shaped molecule was designed and synthesized by covalently incorporating a hexathiobenzene core and a multiple (+)-α-lipoiate group, which can serve as a highly efficient chiral self-assembly initiator,[10] into a unimolecular platform by amide groups (compound **1**, see Figure 1). In this way, this molecular design

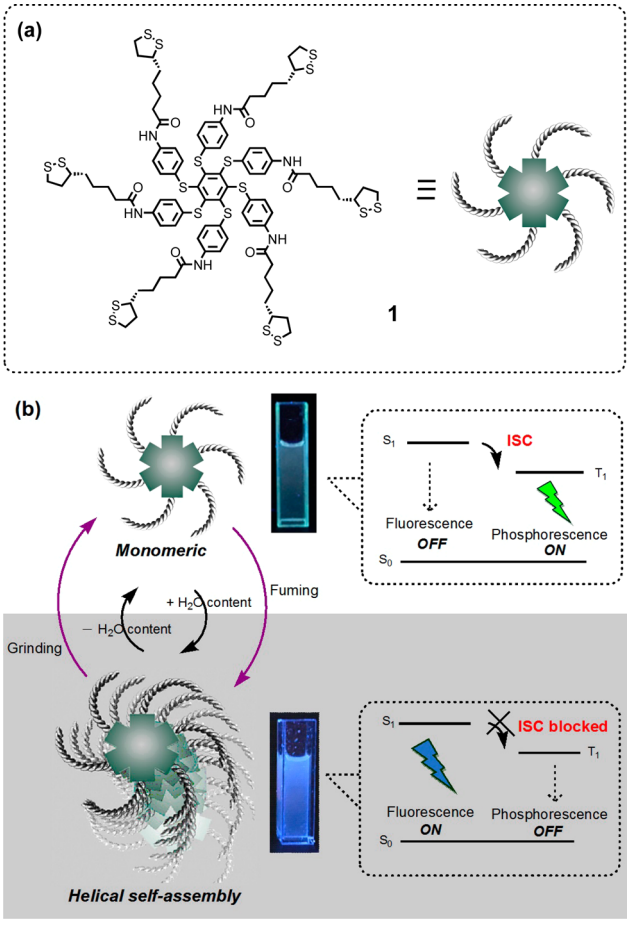

Figure 1. (a) Chemical structures of compound **1**. (b) Schematic representation of a proposed formation and dissociation of the helical assembly of **1** in mixed DMF/H_2O solution or under mechanical stimuli: the monomeric state can give rise to green phosphorescence through an effective ISC process, whereas the aggregated one produces blue fluorescence when the ISC process is blocked by the helical self-assembly.

can take advantage of the competitive effect of multiple intermolecular hydrogen bonding and chirality-driven $\pi-\pi$ stacking to produce a helical conformation, allowing the control of excited-state properties and ISC process for fluorescence-phosphorescence switching.

The synthetic route for the preparation of **1** is outlined in the Experimental Section and Supporting Information (SI). The intermediate compounds **1-2** and **1-3**, and a structurally similar amide-functionalized asterisk molecule **2**, were used as reference molecules for control studies. Mechanical stimuli have attracted much attention in organic optoelectronics since such a tuning approach can be easily imposed on crystal or bulk samples for luminescent applications.[11] In our current design, mechanical stimuli was also employed as an in situ tuning way to allow the emissive switching which can be manipulated in the solid state, accompanied by an analogous helical self-assembly formation and dissociation. Owing to such an efficient S−T interconversion approach, the leading materials can give birth to strong emissions with distinctly pure luminescent tones for the benefit of emitting events.

RESULTS AND DISCUSSION

Switching between Fluorescence and Phosphorescence in Solution. The photophysics of the self-assembly of these compounds was first investigated in DMF/H_2O solution with different water fractions since they have good solubility in DMF but poor solubility in water. As seen from Figure 2a,

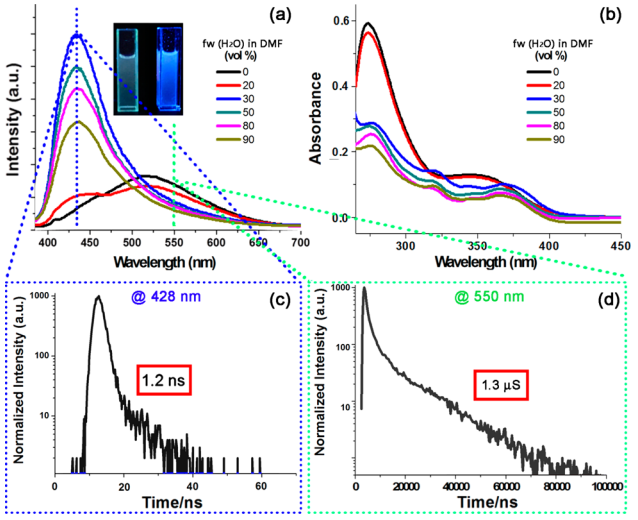

Figure 2. Switching between fluorescence and phosphorescence in solution: (a) Emission spectra upon 365 nm excitation and (b) absorption of **1** in DMF/H_2O with different water fractions. The inset in (a) shows the photographs of **1** in pure DMF and in DMF with 30% water under a UV light (365 nm). Photoluminescent lifetime of **1** upon excitation at 345 nm in nitrogen atmosphere (c) in DMF with 30% water measured at 428 nm and (d) in pure DMF measured at 550 nm emission.

compound **1** shows a modest green emission around 520 nm. However, when the water fraction reached 30%, the emission band were significantly blue-shifted to give rise to a strong blue emission band (~428 nm). Such an emission wavelength shift is extremely remarkable ($\Delta\lambda$ > 90 nm). Correspondingly, the solution luminescent colors are also clearly distinguishable under UV light (see inset of Figure 2a). The Commission Internationale de l'Eclairege (CIE) color coordinate of the emission spectrum of the mixed solution with 30% water was calculated to be (0.18, 0.14), which is in the blue emission region, totally different from the region calculated from the emission of **1** in pure DMF (0.28, 0.41) (Figure S2). When the water fraction continued to increase, the blue luminescent band

DOI: 10.1021/jacs.6b10550
J. Am. Chem. Soc. 2017, 139, 785−791

no longer shifts, showing only a little bit of intensity variation. The quantum yields of **1** in pure DMF solution (1.3%) and in DMF with 30% water (5.4%) can also be obtained, respectively, relative to the standard reference (Rhodamine B, Φ = 65%).

The absorption band of **1** split into several small bands from 300 to 400 nm upon increasing the water fraction in DMF (Figure 2b), due to an aggregation induced alteration of energy levels (see more details vide infra). The changing order in the absorbance is identical with respect to the order in emission. Herein, the conventional H-aggregation and J-aggregation could be ruled out during this process. Therefore, we can infer for this single luminophore that a peculiar excited-state regulation process occurs upon the self-assembly of **1** with the variation of the solvent condition. To further study this unique phenomenon, we collected the photoluminescent (PL) lifetime of each band for compound **1**. Interestingly, we found that a short lifetime of 1.2 ns for the band of 428 nm appeared in DMF with 30% water, as opposed to a relatively long lifetime of 1.3 μs for the band of 550 nm emitted from pure DMF solution (see Figure 2c,d), since the singlet and triplet excited states in the multiamide contained molecule can be stabilized by polarity environment in DMF at room temperature. Such a S−T emissive switching can be further evidenced by low-temperature time-resolved emission measurements (Figure S3). Because the relevant competitive deactivation pathways were greatly suppressed at 77 K, the lifetime of the triplet emission (phosphorescence) can be largely extended into the millisecond scale (2.76 ms), whereas the lifetime of the singlet emission (fluorescence) can be well maintained at the nanosecond scale.[12] These results clearly suggest a fluorescence band and a phosphorescence band, respectively, originating from different solvent conditions. According to relevant literature,[8] the phosphorescence can be confirmed as the hexathiobenzene core is a typical room-temperature phosphorescence emitter. Therefore, it can be concluded that a unique aggregation factor implies the phosphorescence-to-fluorescence conversion. This excited-state regulation process is thus solvent-dependent and accompanied by the switching between monomeric and aggregated states.

Helical Self-Assembly. To further explore the possible self-assembly pathways, transmission (TEM) and scanning electronic microscopy (SEM) were employed to study the aggregated morphologies. According to the literature,[13] the hydrogen bonding between amide groups of **1** and water will mediate the intermolecular H-bond formation, so as to cause the establishment of the helical self-assembled aggregates in organic media with a certain proportion of the water. The helices started to form in DMF with 20% water (Figure 3a), and the nanoarchitectures turned to be perfect when the water fraction reached 30% (see the representative aggregates with an average cross-sectional diameter of 400 nm in Figure 3b). Such a result is in good agreement with the abrupt shown in the optical spectra (Figure 2a,b), namely, featuring a significant phosphorescence-to-fluorescence conversion in DMF with 30% water. However, further increase of water content in the system will shorten the average length of the nanohelices (Figure 3c,d) and resulted in the reduction of the fluorescent intensity (see Figure 2a). There was little chance to form aggregates with small number of units in our system as proven by a series of concentration dependent optical and NMR studies (see Figures S4−S6).

These morphologies revealed clear helically self-assembled nanostructures when observed from SEM (Figure 4a). In addition, the helical stacking modes always appear in a P-helicity fashion. Such a chiral amplification can also be well reflected by circular dichroism (CD) signals. Strong positive−negative−positive Cotton effects, corresponding to the electronic transition of the hexathiobenzene unit and indicating the P-helicity,[14] were observed in mixed DMF/H_2O solution of **1** (Figure 4b). Since no CD signal was observed from the achiral hexathiobenzene chromophore itself, this phenomenon indicates that the macrochirality of the achiral core emerges upon the formation of the helically self-assembled nanostructures driven by the multiple chiral lipoiate groups.

To gain further insight into the fine superstructures of the helical self-assembly from the monomeric state and the aggregated one, we employed molecular dynamics (MD)

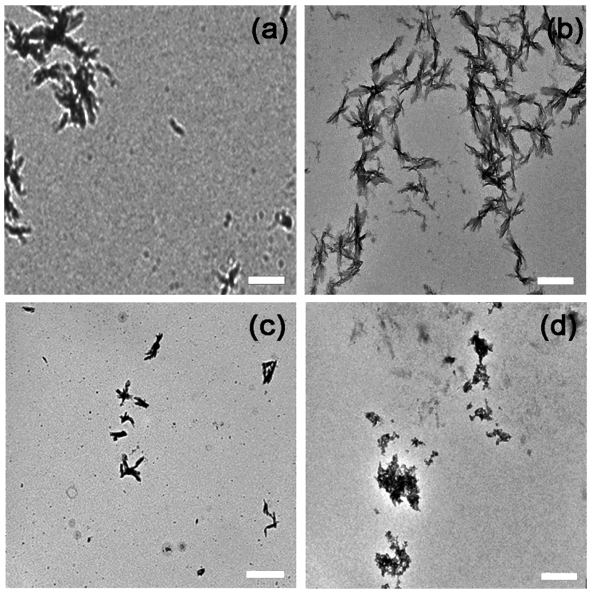

Figure 3. Helical self-assembly: TEM images of **1** prepared from (a) DMF with 20% water, (b) DMF with 30% water, (c) DMF with 50% water, and (d) DMF with 90% water. Scale bar: 1 μm.

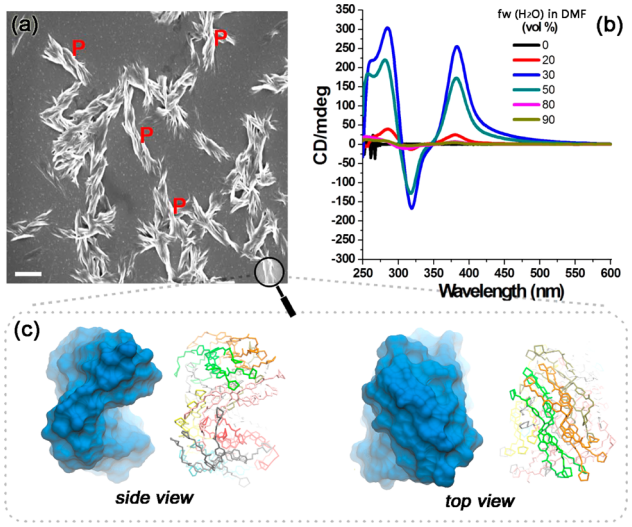

Figure 4. Optical activity: (a) SEM image of **1** prepared from DMF with 30% water (scale bar: 1 μm). Some clear helical twists of the nanostructures are highlighted. (b) CD spectra of **1** in DMF/H_2O with different water fractions. (c) Snapshots of self-assembly conformation of **1** observed from molecular dynamics simulations.

DOI: 10.1021/jacs.6b10550
J. Am. Chem. Soc. 2017, 139, 785−791

simulations[15] to study the aggregation behavior of **1**. It was found that the molecules of **1** quickly formed aggregates when exposed to an aqueous environment (Figure S7), as evidenced by the decrease of the solvent-accessible surface area with respect to simulation time (Figure S8). Although it took different time to reach the aggregation equilibrium from different setups (Figure S8), the van der Waals (VDW) interaction potential energies indicated a similar aggregate conformation via non-covalent interactions (Figure S9). It can be seen from the optimized conformation in Figure 4c that the layer-by-layer hierarchical superstructure occurs via the synergy of the chirality-driven $\pi-\pi$ stacking of the hexathiobenzene core and the hydrogen-bonding alternation of the amide group, indicative of the potential of forming advanced helical architectures through further extension of the twisting force (Figure 4a).[16] From these results, we can conclude that the helical self-assembly of **1** induced the phosphorescence-to-fluorescence conversion. In contrast, the reference compounds **1-2** and **1-3** and compound **2** can only partially cause the triplet-singlet emission transfer (reflected from those dual emission curves in Figure S10), simply due to the fact that they form less ordered aggregates in the mixed DMF/H_2O solution, depending on their chemical structures (Figure S11).

Proposed Mechanism of the Singlet−Triplet Emissive Switching. Having established the helical self-assembling, we proceed to investigate the underlying mechanism of the S−T emission switching of **1**. As compared with the smooth curve in the excitation spectra of the monomeric state, splitted signals of **1** in its helically assembled state was observed (Figure 5a),

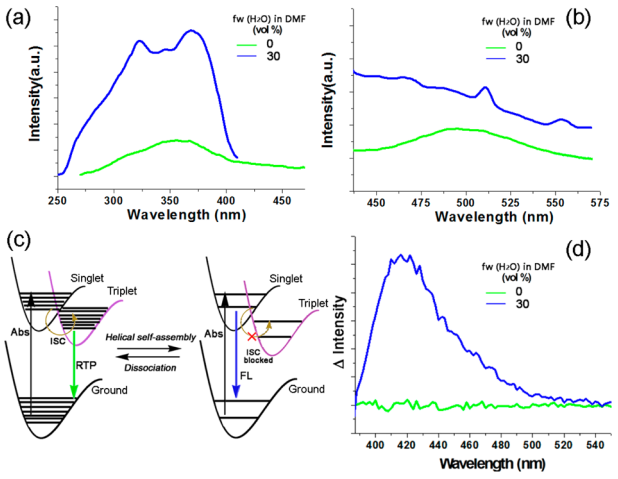

Figure 5. Proposed mechanism of the singlet−triplet emissive switching: (a) Excitation spectra of **1** in pure DMF and in DMF with 30% water collected from 550 and 428 nm, respectively. (b) Emission spectra upon 330 nm excitation of **1** in pure DMF and in DMF with 30% water at 77 K. (c) Schematic representation to describe the switching between phosphorescence and fluorescence of **1** by a reversible blocking of ISC process. (d) CPL spectrum of **1** in DMF/H_2O with 30% water.

similar to the absorption spectral behaviors (Figure 2b). Since the persulfurated aromatic compound is a typical internal charge transfer (ICT) molecule (see the photoluminescence sensitive to solvent polarity (Figure S12) and referenced from relevant reports[17]), the S−T energy gap will alter from room temperature to 77 K.[18] In that case, partial splitted phosphorescent band of **1** can still be observed in DMF with 30% water (Figure 5b). These splitted spectral signals in Figure 5a indicate a discontinuous distribution of local excited (LE), ICT and $\pi-\pi^*$ transitions within a certain vibrational interval of the excited states.[19] Considering that the ISC for triplet-state radiative decay largely relies on the overlap of the vibrational levels of the excited states,[20] the discontinuousness of these levels will disturb the ISC process for producing the phosphorescence. Meanwhile, the outstanding LE and intermolecular $\pi-\pi^*$ bands resulted from the suppression of vibrations of monomer in ICT progress further enlarge the S−T energy gap, which is also unfavorable for ISC.[19]

In addition, we also obtained molecular vibrational information on the self-assemblies of **1** by FT-IR from perspective of electronic ground state. It was found that the vibrational peaks (e.g., $V_{\text{-Ph-S-}}$, $V_{\text{-C=C-}}$, and $V_{\text{-C=O}}$, etc.) of the sample obtained from pure DMF were relatively strong and sharp as compared with those weak and broad ones from DMF with 30% water (Figure S13). These results suggest a vibration-restricted effect of the helical assembly. In terms of the above photophysical studies, a mechanism for the helical self-assembly induced switching between phosphorescence and fluorescence can be proposed (see Figure 5c). For the monomeric state of 1, the electron at ground state has chances to migrate to the vibrational levels of singlet states which are overlapping with those of triplet states. Hence the ISC process is active followed by the phosphorescence decay. Upon the helical self-assembly, however, the molecular vibrations are discontinuously distributed and S−T energy gap is enlarged. Consequently, the ISC process was easily blocked to give rise to fluorescence instead of phosphorescence. Overall, the switchable S−T emissive behavior induced by helical self-assembly can be clearly illustrated in Figure 1b.

Circularly polarized luminescence (CPL) directly proved the relationship between the emissive switching and the supramolecular chirality, as CPL signal tells the excited-state information in a chiroptical environment.[21] As shown in Figure 5d, a CPL signal was found in mixed DMF/H_2O solution of **1**. Since the location of this signal is in accordance with the wavelength of fluorescent band in Figure 2a, we can conclude that the appearance of fluorescence in this system unambiguously resulted from the establishment of the supramolecular chirality. On the contrary, although the molecule produces a phosphorescence in its free state in DMF, no CPL signal was found due to the lack of chiroptical environment (Figure 5d).

Mechanically Induced Luminescent Color Switching. Solid-state emissive organic materials are more popular for practical thin-film-device applications.[22] The solid-state emission property of **1** based on helical self-assembly is very sensitive to mechanical stimuli. As shown in Figure 6b, the fluorescent peak at 428 nm underwent a remarkable red-shift during grinding. As a result, to our delight, the luminescent color conversion of 1 occurred from blue to green after grinding for different time (see Figure 6a). The quantum yield of a solid sample of **1** decreased from 4.6% to 1.5% upon grinding. The changes in the emission of **1** during the grinding process are found to be similar to the emissive switching in DMF/H_2O with variation of water fractions, and the helical morphology (Figure S14) and the PL lifetime change (Figures S15 and S16) can also be clearly characterized. Hence we can deduce that such a mechanistic conversion of multicolor luminescence originates from disintegration of the helical aggregates upon grinding.

Interestingly, such a mechanoluminescent behavior can be recovered by fuming. The solid-state CD spectra of the pristine,

DOI: 10.1021/jacs.6b10550
J. Am. Chem. Soc. 2017, 139, 785−791

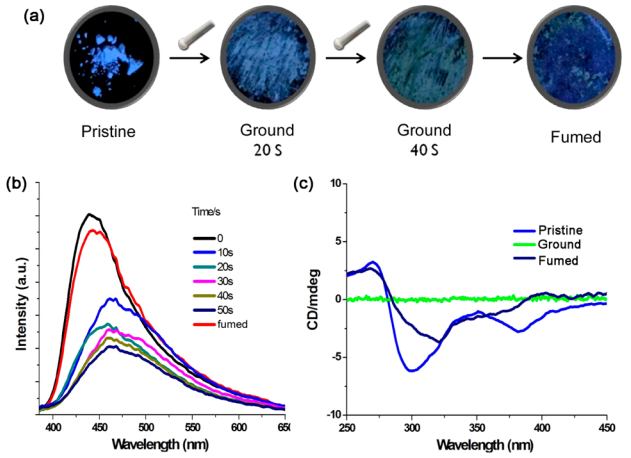

Figure 6. Mechanically induced luminescent color switching: (a) Photographs under UV light (365 nm) and (b) emission spectra upon 365 nm excitation of a solid sample of **1** prepared from DMF with 30% water during the grinding process. (c) Solid-state CD spectra of the pristine and ground films of **1**.

grinded and fumed forms of the solid sample (Figure 6c) were investigated accordingly. The strong Cotton effect of the pristine sample was a representative property of the helically self-assembled samples. The CD signal completely vanished after grinding, indicating an amorphous nature. These CD peaks restored after the sample was fumed in DMF with 30% water vapor (170 °C, in vacuum), suggesting regeneration of the supramolecular chirality in the solid state. The reversible mechanoluminescent color conversion is accompanied by recovery of the emission spectra, revealing a successful switching of the solid-state emissive material.

CONCLUSION

In summary, we have employed supramolecular chirality to design organic functional molecules with a regulation of singlet and triplet emissive properties. Switching between fluorescence and phosphorescence at the unimolecular level was achieved based on the formation and dissociation of helical self-assembly, whereby the competitive effects of multiple intermolecular hydrogen bonding and chirality-driven $\pi-\pi$ stacking play key roles. Our system can also be delivered into the solid state and thereby exhibit reversible mechanoluminescent color conversion relying on an analogous molecular self-assembly alternation. We believe that the strategy demonstrated herein can be valuable for interdisciplinary development of supramolecular chiral science for creating intelligent optoelectronic materials.

EXPERIMENTAL SECTION

General. ^{1}H NMR and ^{13}C NMR spectra were measured on a Bruker 400L spectrometer. Mass spectra were measured by using a matrix-assisted laser desorption/ionization time-of-flight mass spectrometer (5800). Absorption spectra were recorded on a Shimadzu 1800 spectrophotometer, while the fluorescent emission spectra were taken with a Edinburgh FLS920 spectrofluorometer. The fluorescence quantum yields of solution and solid powders were measured on QM40 with an integrating sphere (φ 150 mm) from Photo Technology International, Inc. (PTI, USA). The CD spectra were recorded on a Chirascan CD spectrophotometer (Applied Photophysics Ltd., UK). Transmission electron microscopy (TEM) was performed on a Jeol JEM 2100 with an accelerating voltage of 200 kV. The samples were prepared by drop-casting samples onto 300 mesh carbon grids on a copper support. Fourier transform infrared (FTIR) spectra were obtained from a Nicolet 6700 infrared spectrophotometer by single total reflection of diamond with a scan range of 400−4000 cm^{-1}. For FTIR measurements, **1** in pure DMF and in DMF with 30% water were dropped into a hollow groove on the diamond crystal with corresponding solvent condition as background. The photo images were photographed by a Nikon COOLPIX S8000 digital camera. The ground samples were prepared by grinding with similar force using a spoon.

Synthesis of References Compounds ***1-2*** *and* ***1-3***. The preparation for these compounds was similar to procedures described in the literature.[8b]

Synthesis of Compound ***1***. (R)-(+)-1,2-Dithiolane-3-pentanoic acid (618 mg, 3 mmol), HATU (1.14 g, 3 mmol) was dissolved in DMF (5 mL) and stirred for 15 min at a two-necked round-bottom flask under nitrogen, then compound **1-3** (204 mg, 0.25 mmol) and DIPEA (1 mL) were added. The mixture was stirred at rt for 18 h. Water was introduced and the precipitates were filtered to collect the solid sample. The crude compound was then washed by water, EA, ethanol, acetone to obtained a powder one (200 mg, 41%). ^{1}H NMR (400 MHz, DMSO-d_6, 298 K): δ = 1.39 (m, 6H), 1.64 (m, 24H), 1.88 (m, 6H), 2.38 (m, 18H), 3.15 (m, 6H), 3.63 (m, 6H), 7.15 (d, J = 8.0 Hz, 12H), 7.51 (d, J = 8.0 Hz, 12H), 9.91 (S, 6H). ^{13}C NMR (100 MHz, DMSO-d_6, 298 K): δ = 171.61, 138.94, 129.97, 128.87, 127.78, 120.38, 56.54, 39.34, 38.58, 36.71, 34.64, 28.83, 25.28. MS: MALDI-ToF MS, m/z: [M + H]$^+$ calcd for $C_{42}H_{36}N_6S_6$, 1994.33; found m/z, 1381.23 (m-3*190, m-3*(*R*)-5-(1,2-dithiolan-3-yl) pentanal, fragment peak).

Synthesis of Compound ***2***. 2-(Dimethylamino)acetamide (306 mg, 3 mmol) and HATU (1.14 g, 3 mmol) were dissolved in DMF (5 mL) and stirred for 15 min in a two-necked round-bottom flask under nitrogen, and then compound **1-3** (204 mg, 0.25 mmol) and DIPEA (1 mL) were added. The mixture was stirred at rt for 18 h. Water was introduced, and the precipitates were filtered to collect the solid sample. The crude compound was then washed by water, EA, ethanol, and acetone to obtained a powder (150 mg, 49%). ^{1}H NMR (400 MHz, DMSO-d_6, 298 K): δ = 2.26 (S, 36H), 3.06 (S, 12H), 7.16 (d, J = 8.0 Hz, 12H), 7.60 (d, J = 8.0 Hz, 12H), 9.78 (S, 6H). ^{13}C NMR (100 MHz, DMSO-d_6, 298 K): δ = 167.59, 147.72, 129.30, 142.55, 130.31, 128.57, 126.98, 61.09, 14.31. MS: MALDI-ToF MS, m/z: [M + H]$^+$ calcd for $C_{42}H_{36}N_6S_6$, 1326.39; found m/z, 986.36 (m-4*87, m-4* 2-(dimethylamino)acetaldehyde, fragment peak).

Self-Assemblies in Solution. Compound **1** or **2** (6 mg) was dissolved in DMF (10 mL) and the solution was divided into 10 parts (each 1 mL), followed by addition into DMF and water to obtain a variety of different proportions. TEM, UV/vis, and PL were used for the analysis of the solutions.

Preparation of Solid-State Sample with Blue Luminescence of Compound ***1***. Compound **1** (3 mg) was dissolved in DMF (6 mL) and water (4 mL), and then the above solution was dropcasted onto a clean glass substrate. The solvent was removed by placing at 50 °C and in vacuum for 24 h.

Circular Dichroism. The CD spectra of the samples in solution and in solid state were measured using the settings: wavelength range: 250 nm -600 nm, wavelength increment: 1 nm, bandwidth: 1 nm, time-per-point: 1.0 s, temperature: 20 °C, cell path length: 10 mm, repeat spectra: 3.

Circularly Polarized Luminescence. The CPL spectra of the samples in the two conditions were measured using the settings: excitation wavelength: 365 nm, excitation bandwidth: 16 nm, scanning range: 386−550 nm, wavelength increment: 2 nm, bandwidth: 8 nm, time-per-point: 10 s, temperature: 20 °C, cell path length: 10 mm, repeat spectra: 4.

Computational Details. The geometry of compound **1** was optimized by density functional theory (DFT) calculations using the hybrid B3LYP functional[23] and the double-ζ 6-31G(d) basis set.[24] The electrostatic potential of **1** was calculated at the HF/6-31G(d) level of theory, from which partial atomic charges were derived according to the restrained electrostatic potential (RESP)[25] procedure. The bonded and nonbonded parameters were adopted from the general Amber

DOI: 10.1021/jacs.6b10550
J. Am. Chem. Soc. 2017, 139, 785−791

force field (GAFF).[26] MD simulations of **1** were conducted in aqueous solutions using the GROMACS program package.[27] Two starting structures were generated for 10 molecules of **1** in a cubic box of dimension 10 × 10 × 10 nm^3; the first structure consists of randomly distributed **1** molecules, while the second one is a structure of stacked **1** molecules. Both starting structures were solvated by around 32 000 water molecules and subject to 100 ns MD simulations under ambient temperature and pressure.

■ ASSOCIATED CONTENT

Supporting Information

The Supporting Information is available free of charge on the ACS Publications website at DOI: 10.1021/jacs.6b10550.

Synthesis, characterization, and spectroscopic properties, including Figures S1−S17 (PDF)

■ AUTHOR INFORMATION

Corresponding Authors

*qz14@sjtu.edu.cn

*zhuliangliang@fudan.edu.cn

ORCID

Liangliang Zhu: 0000-0001-6268-3351

Notes

The authors declare no competing financial interest.

■ ACKNOWLEDGMENTS

This work was supported by the NSFC/China (21644005) and National Program for Thousand Young Talents of China. X.L. and H.Å. thank the Swedish National Infrastructure for Computing (SNIC) for providing computational resources for project SNIC 2014-11/31. H.W. and L.Z. thank Dr. G. Liu for helpful discussions and Applied Photophysics Ltd (UK) for assistance with the CPL studies.

■ REFERENCES

(1) (a) Joyce, G. F. *Nature* **2002**, *418*, 214. (b) Valev, V. K.; Baumberg, J. J.; Sibilia, C.; Verbiest, T. *Adv. Mater.* **2013**, *25*, 2517. (c) Edwards, W.; Smith, D. K. *J. Am. Chem. Soc.* **2014**, *136*, 1116. (d) Zhou, Y.; Yang, M.; Sun, K.; Tang, Z.; Kotov, N. A. *J. Am. Chem. Soc.* **2010**, *132*, 6006. (e) Mateos-Timoneda, M. A.; Crego-Calama, M.; Reinhoudt, D. N. *Chem. Soc. Rev.* **2004**, *33*, 363. (f) Lehn, J.-M. *Science* **2002**, *295*, 2400−2403. (g) Qiu, H.; Che, S. *Chem. Soc. Rev.* **2011**, *40*, 1259. (h) Li, Z.; Zhu, Z.; Liu, W.; Zhou, Y.; Han, B.; Gao, Y.; Tang, Z. *J. Am. Chem. Soc.* **2012**, *134*, 3322. (i) Smith, D. K. *Chem. Soc. Rev.* **2009**, *38*, 684. (j) de Jong, J. J. D. D.; Lucas, L. N.; Kellogg, R. M.; van Esch, J. H.; Feringa, B. L. *Science* **2004**, *304*, 278. (k) Wolffs, M.; George, S. J.; Tomovic, Z.; Meskers, S. C.; Schenning, A. P.; Meijer, E. W. *Angew. Chem., Int. Ed.* **2007**, *46*, 8203.

(2) (a) Murata, K.; Aoki, M.; Suzuki, T.; Harada, T.; Kawabata, H.; Komori, T.; Ohseto, F.; Ueda, K.; Shinkai, S. *J. Am. Chem. Soc.* **1994**, *116*, 6664. (b) Gopal, A.; Hifsudheen, M.; Furumi, S.; Takeuchi, M.; Ajayaghosh, A. *Angew. Chem., Int. Ed.* **2012**, *51*, 10505. (c) Shen, Z.; Jiang, Y.; Wang, T.; Liu, M. *J. Am. Chem. Soc.* **2015**, *137*, 16109. (d) Stals, P. J. M.; Korevaar, P. A.; Gillissen, M. A. J.; de Greef, T. F. A.; Fitie, C. F. C.; Sijbesma, R. P.; Palmans, A. R. A.; Meijer, E. W. *Angew. Chem., Int. Ed.* **2012**, *51*, 11297. (e) Cui, J.; Lu, X.; Liu, A.; Wan, X.; Zhou, Q. *Macromolecules* **2009**, *42*, 7678.

(3) (a) Aida, T.; Meijer, E. W.; Stupp, S. I. *Science* **2012**, *335*, 813. (b) Chen, C. L.; Rosi, N. L. *Angew. Chem., Int. Ed.* **2010**, *49*, 1924. (c) Zhu, J.; Peng, H.; Marshall, A. F.; Barnett, D. M.; Nix, W. D.; Cui, Y. *Nat. Nanotechnol.* **2008**, *3*, 477. (d) Liu, G.; Zhang, D.; Feng, C. *Angew. Chem., Int. Ed.* **2014**, *53*, 7789. (e) van Dijken, D. J.; Beierle, J. M.; Stuart, M. C.; Szymanski, W.; Browne, W. R.; Feringa, B. L. *Angew. Chem., Int. Ed.* **2014**, *53*, 5073. (f) Yang, Y.; Zhang, Y.; Wei, Z. *Adv. Mater.* **2013**, *25*, 6039−6049.

(4) (a) Li, G. J.; Fleetham, T.; Li, J. *Adv. Mater.* **2014**, *26*, 2931. (b) Yang, Q. Y.; Lehn, J. M. *Angew. Chem., Int. Ed.* **2014**, *53*, 4572. (c) Zhu, L.; Li, X.; Zhang, Q.; Ma, X.; Li, M.; Zhang, H.; Luo, Z.; Ågren, H.; Zhao, Y. *J. Am. Chem. Soc.* **2013**, *135*, 5175.

(5) (a) Reineke, S.; Seidler, N.; Yost, S. R.; Prins, F.; Tisdale, W. A.; Baldo, M. A. *Appl. Phys. Lett.* **2013**, *103*, 093302. (b) Gong, Y. Y.; Zhao, L. F.; Peng, Q.; Fan, D.; Yuan, W. Z.; Zhang, Y. M.; Tang, B. Z. *Chem. Sci.* **2015**, *6*, 4438.

(6) (a) Liu, Y.; Nishiura, M.; Wang, Y.; Hou, Z. *J. Am. Chem. Soc.* **2006**, *128*, 5592. (b) Sakai, A.; Tanaka, M.; Ohta, E.; Yoshimoto, Y.; Mizuno, K.; Ikeda, H. *Tetrahedron Lett.* **2012**, *53*, 4138.

(7) (a) Tucker, H. R.; Gingras, M.; Brand, H.; Lehn, J. M. *J. Chem. Soc., Perkin Trans. 2* **1997**, 1303. (b) Gingras, M.; Raimundo, J. M.; Chabre, Y. M. *Angew. Chem., Int. Ed.* **2006**, *45*, 1686.

(8) (a) Fermi, A.; Bergamini, G.; Roy, M.; Gingras, M.; Ceroni, P. *J. Am. Chem. Soc.* **2014**, *136*, 6395. (b) Wu, H.; Hang, C.; Li, X.; Yin, L.; Zhu, M.; Zhang, J.; Zhou, Y.; Ågren, H.; Zhang, Q.; Zhu, L. *Chem. Commun.* **2017**, DOI: 10.1039/C6CC04901J.

(9) (a) Adams, R.; Ferretti, A. *J. Am. Chem. Soc.* **1959**, *81*, 4927. (b) Sleiman, M.; Varrot, A.; Raimundo, J. M.; Gingras, M.; Goekjian, P. G. *Chem. Commun.* **2008**, 6507.

(10) (a) Zhu, L.; Li, X.; Wu, S.; Nguyen, K. T.; Yan, H.; Ågren, H.; Zhao, Y. *J. Am. Chem. Soc.* **2013**, *135*, 9174. (b) Zhu, L.; Yan, H.; Nguyen, K. T.; Tian, H.; Zhao, Y. *Chem. Commun.* **2012**, *48*, 4290.

(11) (a) Chan, E. P.; Walish, J. J.; Urbas, A. M.; Thomas, E. L. *Adv. Mater.* **2013**, *25*, 3934. (b) Sagara, Y.; Kato, T. *Angew. Chem., Int. Ed.* **2008**, *47*, 5175. (c) Xu, B.; Mu, Y.; Mao, Z.; Xie, Z.; Wu, H.; Zhang, Y.; Jin, C.; Chi, Z.; Liu, S.; Xu, J.; Wu, C. Y.; Lu, P. Y.; Lien, A.; Bryce, M. R. *Chem. Sci.* **2016**, *7*, 2201. (d) Gong, Y.; Chen, G.; Peng, Q.; Yuan, W.; Xie, Y.; Zhang, Y. M.; Tang, B. Z. *Adv. Mater.* **2015**, *27*, 6195. (e) Xie, Z.; Chen, C.; Xu, S.; Li, J.; Zhang, Y.; Liu, S.; Xu, J.; Chi, Z. *Angew. Chem., Int. Ed.* **2015**, *54*, 7181.

(12) Zhu, L. L.; Trinh, M. T.; Yin, L. Y.; Zhang, Z. Y. *Chem. Sci.* **2016**, *7*, 2058.

(13) Liu, C. X.; Jin, Q. X.; Lv, K.; Zhang, L.; Liu, M. H. *Chem. Commun.* **2014**, *50*, 3702.

(14) (a) Berova, N.; Bari, L. D.; Pescitelli, G. *Chem. Soc. Rev.* **2007**, *36*, 914. (b) Canary, J. W. *Chem. Soc. Rev.* **2009**, *38*, 747.

(15) (a) Cai, Y.; Guo, Z.; Chen, J.; Li, W.; Zhong, L.; Gao, Y.; Jiang, L.; Chi, L.; Tian, H.; Zhu, W. H. *J. Am. Chem. Soc.* **2016**, *138*, 2219. (b) Danila, I.; Riobé, F.; Piron, F.; Puigmartí-Luis, J.; Wallis, J. D.; Linares, M.; Ågren, H.; Beljonne, D.; Amabilino, D. B.; Avarvari, N. *J. Am. Chem. Soc.* **2011**, *133*, 8344.

(16) (a) Li, X.; Zhu, L.; Duan, S.; Zhao, Y.; Ågren, H. *Phys. Chem. Chem. Phys.* **2014**, *16*, 23854. (b) Zhu, L.; Li, X.; Sanders, S. N.; Ågren, H. *Macromolecules* **2015**, *48*, 5099.

(17) (a) Bergamini, G.; Fermi, A.; Botta, C.; Giovanella, U.; DiMotta, S.; Negri, F.; Peresutti, R.; Gingras, M.; Ceroni, P. *J. Mater. Chem. C* **2013**, *1*, 2717. (b) Jiang, Y.; Gindre, D.; Allain, M.; Liu, P.; Cabanetos, C.; Roncali, J. *Adv. Mater.* **2015**, *27*, 4285.

(18) (a) Zhang, Q.; Li, J.; Shizu, K.; Huang, S.; Hirata, S.; Miyazaki, H.; Adachi, C. *J. Am. Chem. Soc.* **2012**, *134*, 14706. (b) Xu, S. D.; Yuan, Y. Y.; Cai, X. L.; Zhang, C. J.; Hu, F.; Liang, J.; Zhang, G. X.; Zhang, D. Q.; Liu, B. *Chem. Sci.* **2015**, *6*, 5824.

(19) (a) Haidekker, M. A.; Theodorakis, E. A. *J. Biol. Eng.* **2010**, *4*, 11. (b) Kuimova, M. K. *Phys. Chem. Chem. Phys.* **2012**, *14*, 12671−12686. (c) Yang, Z.; Mao, Z.; Zhang, X.; Ou, D.; Mu, Y.; Zhang, Y.; Zhao, C.; Liu, S.; Chi, Z.; Xu, J.; Wu, Y.-C.; Lu, P.-Y.; Lien, A.; Bryce, M. R. *Angew. Chem., Int. Ed.* **2016**, *55*, 2181.

(20) (a) Leitl, M. J.; Krylova, V. A.; Djurovich, P. I.; Thompson, M. E.; Yersin, H. *J. Am. Chem. Soc.* **2014**, *136*, 16032. (b) Tilley, A. J.; Pensack, R. D.; Lee, T. S.; Djukic, B.; Scholes, G. D.; Seferos, D. S. *J. Phys. Chem. C* **2014**, *118*, 9996.

(21) (a) Kim, J.; Lee, J.; Kim, W. Y.; Kim, H.; Lee, S.; Lee, H. C.; Lee, Y. S.; Seo, M.; Kim, S. Y. *Nat. Commun.* **2015**, *6*, 6959. (b) Shen, Z.; Wang, T.; Shi, L.; Tang, Z.; Liu, M. *Chem. Sci.* **2015**, *6*, 4267.

(22) (a) Mutai, T.; Satou, H.; Araki, K. *Nat. Mater.* **2005**, *4*, 685. (b) Zhu, L.; Tran, H.; Beyer, F. L.; Walck, S. D.; Li, X.; Ågren, H.; Killops, K. L.; Campos, L. M. *J. Am. Chem. Soc.* **2014**, *136*, 13381.

(c) Li, R.; Xiao, S.; Li, Y.; Lin, Q.; Zhang, R.; Zhao, J.; Yang, C.; Zou, K.; Li, D.; Yi, T. *Chem. Sci.* **2014**, *5*, 3922−3928.
(23) Becke, A. D. *J. Chem. Phys.* **1993**, *98*, 5648−5652.
(24) Hehre, W.; Ditchfield, J. R.; Pople, J. A. *J. Chem. Phys.* **1972**, *56*, 2257−2261.
(25) Bayly, C. I.; Cieplak, P.; Cornell, W.; Kollman, P. A. *J. Phys. Chem.* **1993**, *97*, 10269−10280.
(26) Wang, J.; Wolf, R. M.; Caldwell, J. W.; Kollman, P. A.; Case, D. A. *J. Comput. Chem.* **2004**, *25*, 1157−1174.
(27) Hess, B.; Kutzner, C.; van der Spoel, D.; Lindahl, E. *J. Chem. Theory Comput.* **2008**, *4*, 435−447.

DOI: 10.1021/jacs.6b10550
J. Am. Chem. Soc. 2017, 139, 785−791